Versatile in vivo regulation of tumor phenotypes by dCas9-mediated transcriptional perturbation

Christian J. Braun[a,b,1], Peter M. Bruno[a,b,1], Max A. Horlbeck[c,d,e], Luke A. Gilbert[c,d,e], Jonathan S. Weissman[c,d,e], and Michael T. Hemann[a,b,2]

[a]The David H. Koch Institute for Integrative Cancer Research, Massachusetts Institute of Technology, Cambridge, MA 02139; [b]Department of Biology, Massachusetts Institute of Technology, Cambridge, MA 02139; [c]Department of Cellular and Molecular Pharmacology, California Institute for Quantitative Biomedical Research, University of California, San Francisco, CA 94158; [d]Howard Hughes Medical Institute, University of California, San Francisco, CA 94158; and [e]Center for RNA Systems Biology, University of California, San Francisco, CA 94158

Edited by Lars Zender, Tübingen University, Tübingen, Germany, and accepted by Editorial Board Member Tak W. Mak May 23, 2016 (received for review January 13, 2016)

Targeted transcriptional regulation is a powerful tool to study genetic mediators of cellular behavior. Here, we show that catalytically dead Cas9 (dCas9) targeted to genomic regions upstream or downstream of the transcription start site allows for specific and sustainable gene-expression level alterations in tumor cells in vitro and in syngeneic immune-competent mouse models. We used this approach for a high-coverage pooled gene-activation screen in vivo and discovered previously unidentified modulators of tumor growth and therapeutic response. Moreover, by using dCas9 linked to an activation domain, we can either enhance or suppress target gene expression simply by changing the genetic location of dCas9 binding relative to the transcription start site. We demonstrate that these directed changes in gene-transcription levels occur with minimal off-target effects. Our findings highlight the use of dCas9-mediated transcriptional regulation as a versatile tool to reproducibly interrogate tumor phenotypes in vivo.

cancer genetics | cancer models | cancer therapeutic resistance | gene regulation | CRISPR

Because of the dramatic decline in sequencing costs and the increase in sequencing efficiency over the last decade (1), the amount of descriptive knowledge about the cancer genome and transcriptome has increased exponentially. However, the acquisition of this information has greatly outpaced our capability to functionally study the biological roles of putative cancer genes (2, 3). Determining the relative contribution of an individual gene alteration in the context of the many changes found in a given tumor cell is challenging, as is discriminating cancer-driving mutations from silent ones (4).

The application of nucleases targeted to specific regions of the genome-like zinc finger nucleases (ZFNs) (5, 6), transcription activator-like effector nucleases (7), and clustered regularly interspaced short palindromic repeats (CRISPR) (8, 9) have made it possible to study the functional relevance of specific genomic mutations. Most notably, the CRISPR-associated protein 9 (Cas9) protein can be targeted to genomic regions of interest by easily programmable short guide RNA (sgRNA) molecules. This approach has been used to elegantly study mutational phenotypes (10) and to screen for novel mediators of disease (11–15). However, most genome editing applications are focused on loss-of-function phenotypes caused by genomic frameshift mutations, making it hard to study scenarios in which tumor progression and relapse are driven by gene activation. This is particularly true for mechanisms leading to resistance to cancer treatment, where a gene transcript level may increase by gene amplification (16–20) or mere up-regulation (21, 22), which can lead to potent resistance phenotypes, ultimately resulting in treatment failure and patient death. In contrast to transcriptional inactivation, large-scale gene overexpression studies are technically challenging, costly, and do not allow for a rapid and flexible pooled library construction (23), underlining the necessity to develop novel tools amenable for rapid modeling of gene activation phenotypes.

Catalytically inactive, or dead, Cas9 (dCas9), with its potential to either activate or inactivate the transcription of specific genes, has recently emerged as an alternative to genome editing, RNA interference, and cDNA overexpression. sgRNA molecules are used to specifically target dCas9, with or without linked effector molecule domains, to genomic regions of interest. Depending on the targeted genomic region and on the effector molecule domain, dCas9 can then either cause transcriptional repression or activation. Whereas the transcriptional perturbation mediated by dCas9 has efficiently been used to study in vitro phenotypes in tissue culture cells (24–31), evidence for long-term sustained in vivo activity and for the feasibility of in vivo gene repression/activation screens is still lacking. One of the biggest challenges for achieving this goal is that dCas9 has to be constantly expressed to mediate its inhibitory or activating effects on transcription. This necessity stands in sharp contrast to applications of catalytically active Cas9, where, theoretically, a short duration of Cas9 expression may be enough to create irreversible mutations.

Here, we describe the development and application of a dCas9-based system capable of long-lasting transcriptional repression and activation in vitro and in vivo in multiple immune-competent mouse models of cancer. Additionally, to our knowledge, we present the first in vivo multiplexed gene activation screen for mediators of bone marrow treatment relapse in a syngeneic mouse model for acute lymphoblastic leukemia (ALL). We demonstrate that this technology is fully amenable to model the functional consequences of transcriptional changes found in human cancers.

Significance

Tumor development is accompanied by widespread genomic and transcriptional changes. The mere acquisition of this information has greatly outpaced our capability to functionally study the biological roles of altered genes. This dilemma highlights the necessity to develop technologies that facilitate a rapid functional prioritization among lists of altered genes. Here, we use catalytically dead Cas9 to specifically activate or inactivate the transcription of genes in mouse models of cancer. This approach allows us to study the impact of gene-level changes in vivo and to systematically screen for novel genetic mediators of treatment relapse. We expect that this approach can be used to systematically dissect the biological role of cancer-related genes, a process critical to identifying new cancer drug targets.

Author contributions: C.J.B., P.M.B., L.A.G., and M.T.H. designed research; C.J.B. and P.M.B. performed research; C.J.B., P.M.B., M.A.H., L.A.G., and J.S.W. contributed new reagents/analytic tools; C.J.B. and P.M.B. analyzed data; and C.J.B., P.M.B., and M.T.H. wrote the paper.

The authors declare no conflict of interest.

This article is a PNAS Direct Submission. L.Z. is a guest editor invited by the Editorial Board.

[1]C.J.B. and P.M.B. contributed equally to this work.

[2]To whom correspondence should be addressed. Email: hemann@mit.edu.

This article contains supporting information online at www.pnas.org/lookup/suppl/doi:10.1073/pnas.1600582113/-/DCSupplemental.

We show that the transcriptional changes are highly specific and that both gene-induction and gene-inactivation phenotypes can be achieved by specific genomic targeting of the same dCas9 construct.

Results

Inhibition of *Trp53* Transcription by dCas9 Leads to a Potent Inactivation of TRP53 Function and Resistance to DNA Damage. CRISPR interference (CRISPRi) can repress transcription either by directly interfering with transcriptional initiation (if targeted to the promoter) or by blocking RNA elongation (if targeted to the first exon of a particular gene) (25, 32). To explore whether this genetic inactivation is potent enough to model genetic changes that occur during cancer progression and the evolution of therapeutic resistance, we coinfected murine Eμ-*Myc* $p19^{Arf-/-}$ lymphoma cells (33) with a retroviral vector-expressing dCas9 and a lentiviral vector expressing specific sgRNAs (Fig. 1 *A* and *B* and *SI Appendix*, Figs. S1 and S2). We screened multiple sgRNAs targeting the genomic area around the transcription start site (TSS) of *Trp53* (Fig. 1*C*), with the goal of using dCas9 as a "roadblock" that blocks transcriptional elongation (Fig. 1*D*). *TRP53* is mutated in more than half of all sporadic cancers, and its activation upon cellular stress can elicit a broad set of cellular responses including cell cycle arrest, cellular senescence, and apoptosis (34–36). Inactivation of TRP53 accelerates oncogene-mediated tumorigenesis (37) and renders cells less sensitive to apoptosis (38). Thus, we first investigated which sgRNAs were best at mediating resistance to DNA damage. To do this, we partially infected Eμ-*Myc* $p19^{Arf-/-}$ cells with both dCas9 and single sgRNAs targeting various places along the *Trp53* gene body. Most sgRNAs were targeted to exon 1, but several others were targeted both upstream and downstream as negative controls. These mixed populations of sgRNA-dCas9 expressing and nonexpressing cells were then treated with the DNA damage agent cisplatin, and the relative composition of sgRNA-dCas9 expressing to nonexpressing cells was assayed via flow cytometry (Fig. 1*E*). We found that all sgRNAs targeting dCas9 to exon 1 of *Trp53* promoted cellular resistance to DNA damage (Fig. 1*F*). In concordance with this result, after cisplatin treatment, TRP53 mRNA and protein up-regulation was also diminished in the presence of

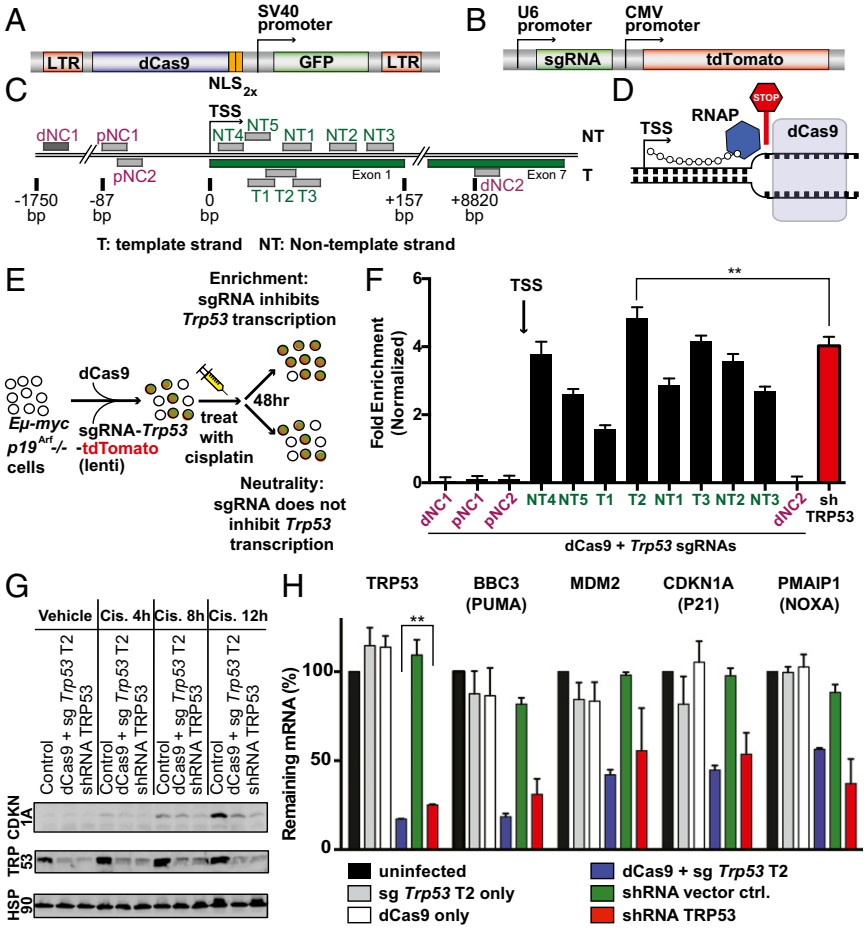

Fig. 1. dCas9 targeted to the TSS of *Trp53* leads to a potent and sustainable loss of TRP53 function. (*A*) A vector diagram of MSCV-dCas9-GFP. (*B*) A vector diagram of U6-sgRNA-tdTomato. (*C*) An overview of sgRNA target sites at the murine *Trp53* locus. dNC, distal negative control, based on their distant location from the TSS. pNC, proximal negative control, based on their relatively close location to the TSS. Green represents sgRNAs predicted to knockdown based on their location in the first exon, just downstream of the TSS. (*D*) Schematic overview of dCas9-mediated interruption of transcriptional elongation by RNA polymerase (RNAP). (*E*) A schematic overview of in vitro competition assays. (*F*) Normalized fold-enrichment of individual sgRNAs targeting different regions of the *Trp53* locus after cisplatin treatment compared with RNAi (shRNA TRP53). No enrichment would lead to a normalized fold enrichment score of zero. $^{**}P < 0.01$ between the two indicated conditions via Student's *t* test. Data are represented as mean ± SEM. (*G*) A Western blot showing a time course of TRP53 and CDKN1A accumulation in Eμ-*Myc* $p19^{Arf-/-}$ lymphoma after cisplatin (Cis.) treatment in control cells and cells with TRP53 down-regulation by either dCas9-mediated transcriptional interference or RNAi. (*H*) qRT-PCR assessment of TRP53 and TRP53 target-gene levels after cisplatin treatment after interfering with TRP53 expression levels. $^{**}P < 0.01$ via Student's *t* test. Data are represented as mean ± SEM.

nearly all of the sgRNAs designed to target genomic DNA within exon 1 (*SI Appendix*, Figs. S3 and S4). In contrast, targeting dCas9 upstream, or far downstream, of the TSS failed to significantly interfere with TRP53 mRNA levels or confer resistance to cisplatin. These assays all demonstrated a similar or bigger impact on TRP53 expression levels and cellular function as the best TRP53 targeting shRNA found by tiling the *TRP53* gene (39). Additionally, we found that dCas9-mediated inactivation had profound effects on TRP53's capability to activate its downstream target genes and in most cases, more so than the TRP53 shRNA (Fig. 1 *G* and *H*).

CRISPRi Is a Potent Tool for Modeling the Genetics of Cancer Progression and Therapeutic Resistance in Vivo. Cas9 is part of the adaptive immune system of *Streptococcus pyogenes* and is not expressed in higher eukaryotes. Thus, if expressed in mammalian systems, the protein might be recognized by a host immune system and lead to adverse responses and graft rejection as recently demonstrated in adenoviral delivery of Cas9 into liver parenchyma (40). Furthermore, an application of dCas9 requires the constant expression of both dCas9 and a sgRNA to enable long-term genetic silencing. To explore the possibility of an in vivo application of dCas9, we tail-vein injected pure populations of Eμ-*Myc p19*$^{Arf-/-}$ cells expressing dCas9 and sgRNAs targeting *Trp53* along with multiple control constructs into syngeneic and fully immunocompetent C57BL/6J mice (Fig. 2*A*). Mice were euthanized upon disease onset and lymphoma cells were isolated from lymph nodes. We then assessed TRP53 mRNA levels by quantitative real-time PCR (qRT-PCR) and observed a strong and consistent repression of TRP53 transcript levels in mice with dCas9 targeted to *Trp53* exon 1 (Fig. 2*B*). This level of TRP53 suppression exceeded the down-regulation seen in vitro and suggested a selection of cells with a more potent inactivation of TRP53 during disease progression. To determine whether this extent of TRP53 loss was significant enough to impact the speed of tumor development and response to chemotherapy, we transplanted Eμ-*Myc p19*$^{Arf-/-}$ cells expressing dCas9 and either a control sgRNA (Gal4) or either of two sgRNAs targeting *Trp53* (T2, T3) into syngeneic C57BL/6J mice (25). Survival analysis revealed that down-regulation of Trp53 by dCas9 is capable of accelerating disease onset (Fig. 2*C*) and significantly reducing overall survival (Fig. 2*D*). Furthermore, repression of Trp53 expression renders cells insensitive to cisplatin treatment in vivo, with overall survival rates indistinguishable from matched control cohorts treated with vehicle alone (Fig. 2*D* and *SI Appendix*, Fig. S5). Thus, dCas9-mediated transcriptional interference is potent, long-lasting, and consistent enough to model the effect of gene suppression on tumor progression. Most importantly, these effects are preserved in vivo despite the presence of a fully functional immune system.

***Mgmt* Transcriptional Activation via dCas9-VP64 Provokes Cellular Resistance to Temozolomide in Vitro and in Vivo.** Given the ability to transcriptionally silence TRP53 both in vitro and in vivo using dCas9, we next wanted to explore the feasibility of CRISPR-mediated gene activation (CRISPRa) in vivo by using a dCas9 fusion to a fourfold repeat of the VP16 transcriptional activator (VP64) (41) (Fig. 3 *A* and *B* and *SI Appendix*, Figs. S6 and S7). We chose to target *Mgmt* (O^6-methylguanine–DNA methyltransferase), a gene encoding a suicide enzyme known to detoxify DNA lesions caused by the chemotherapeutic agent temozolomide (TMZ) (42) (Fig. 3*G*). Epigenetic silencing of the *Mgmt* gene renders cells more sensitive to TMZ, whereas high transcript levels of MGMT are associated with a poor response to TMZ

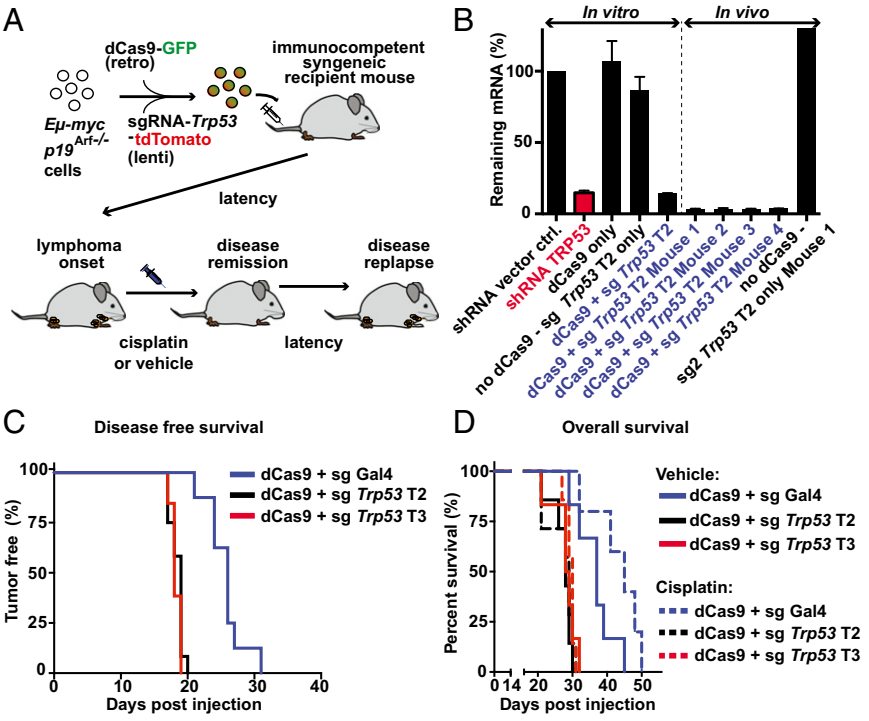

Fig. 2. Transcriptional modulation by dCas9 can alter tumor progression and treatment response in vivo. (*A*) Schematic overview of in vivo lymphoma transplantation experiments into syngeneic C57BL/6J mice. (*B*) TRP53 mRNA levels as assessed by qRT-PCR in vitro and in vivo after dCas9-mediated transcriptional silencing. (*C*) Time to disease onset in the absence of treatment. Via log-rank test $P < 0.0001$ between both Gal4 vs. T2 and Gal4 vs. T3 (mouse numbers: dCas9 + sgGal4 $n = 8$, dCas9 + sg*Trp53* T2 $n = 12$, dCas9 + sg*Trp53* T3 $n = 13$). (*D*) Overall survival with and without silencing of TRP53 and with and without cisplatin treatment. Via log-rank test $P < 0.01$ between both Gal4 vs. T2 and Gal4 vs. T3 (mouse numbers: dCas9 + sgGal4 vehicle $n = 6$, dCas9 + sgGal4 cisplatin $n = 5$, dCas9 + sg*Trp53* T2 vehicle $n = 7$, dCas9 + sg*Trp53* T2 cisplatin, dCas9 + sg*Trp53* T3 vehicle $n = 6$, dCas9 + sg*Trp53* T3 cisplatin $n = 7$).

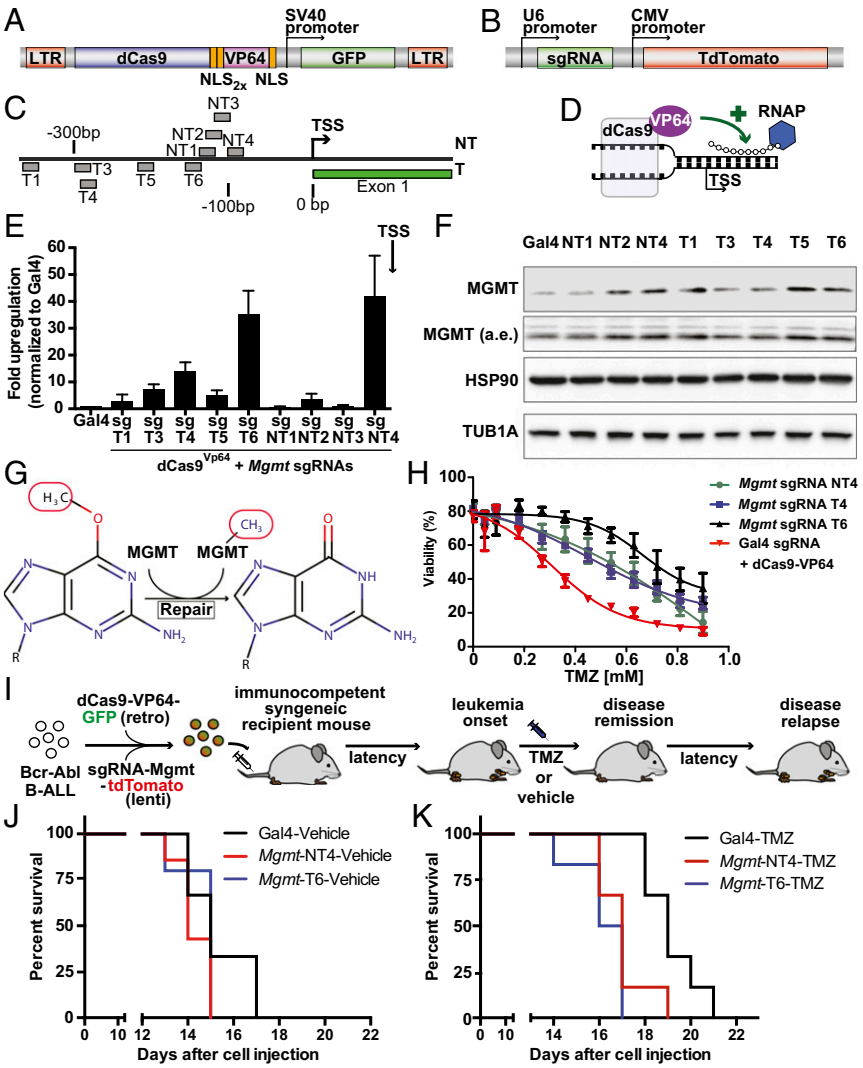

Fig. 3. A fusion of dCas9 with the VP64 activation domain targeted to a genomic region upstream of the TSS of *Mgmt* mediates temozolomide resistance. Plasmid maps of MSCV-dCas9-VP64-GFP (*A*) and U6-sgRNA-tdTomato (*B*). (*C*) A schematic overview of genomic binding sites of sgRNAs targeting murine *Mgmt* upstream of the TSS. (*D*) A schematic showing dCas9-VP64-GFP producing transcriptional activation. (*E*) The fold up-regulation of MGMT mRNA by dCas9-VP64 and multiple sgRNAs normalized to Gal4 negative control assessed by qRT-PCR. Data are represented as mean ± SEM. (*F*) Western blot analysis showing MGMT protein expression after transcriptional activation with different sgRNAs (a.e., alternative exposure). (*G*) A schematic overview of MGMT's enzymatic function. (*H*) A dose–response curve of B-ALL cells treated in vitro with or without transcriptional activation of *Mgmt*. LogIC50's are significantly different at $P < 0.001$ by an extra sum-of-squares *F* test. (*I*) A schematic overview depicting in vivo transplantation of B-ALL cells into syngeneic immune-competent C57BL/6J mice. Kaplan–Meier curves with or without *Mgmt* induction and after vehicle (*J*) ($P = 0.2682$, log rank test) or TMZ treatment (*K*) ($P = 0.0039$, log rank test) (mouse numbers: dCas9 + sgGal4 vehicle $n = 6$, dCas9 + sgGal4 TMZ $n = 6$, dCas9 + sg*Mgmt*-NT4 vehicle $n = 7$, dCas9 + sg*Mgmt*-NT4 TMZ $n = 6$, dCas9 + sg*Mgmt*-T6 vehicle $n = 5$, dCas9 + sg*Mgmt*-T6 $n = 6$).

(43–45). We generated 10 unique sgRNAs targeting the genomic region upstream of *Mgmt*'s TSS (Fig. 3*C*), transduced *Bcr-Abl*–driven murine acute B-cell lymphoblastic leukemia cells (B-ALL) with both dCas9-VP64 and single sgRNAs and analyzed MGMT expression by both qRT-PCR and Western blot. Multiple sgRNAs elicited a robust up-regulation of MGMT at both the mRNA and protein levels (with 7 of 9 sgRNAs having more than twofold, 5 of 9 having more than fivefold, 3 of 9 having more than 10-fold, and 2 of 9 having more than 30-fold up-regulation of MGMT mRNA levels) (Fig. 3 *D*–*F* and *SI Appendix*, Fig. S8). To determine whether the observed gene activation confers protection to TMZ, we performed in vitro drug dosing with TMZ for sgRNAs NT4, T4, and T6. As expected, all three sgRNAs conferred resistance to TMZ (Fig. 3*H*). Additionally, we compared the CRISPRa-mediated induction of MGMT to an MGMT cDNA in terms of both expression and drug resistance. Although both approaches yielded comparable protein expression of MGMT, CRISPRa rendered cells significantly more resistant to TMZ than the cDNA (*SI Appendix*, Fig. S9 *A* and *B*).

We next sought to determine whether CRISPRa could similarly be used to model treatment response in vivo. We therefore transplanted B-ALL cells infected with a combination of dCas9-VP64 and sgRNAs either activating *Mgmt* transcription (NT4, T6) or a nontargeting negative control (Gal4) into syngeneic and fully immune-competent C57BL6/6J mice (Fig. 3*I*). Upon disease manifestation, mice were either treated with TMZ or with vehicle. Whereas the transcriptional activation of *Mgmt* did not have a significant influence on mouse survival in the absence of treatment (Fig. 3*J*), increased expression of MGMT lead to a substantial resistance to TMZ treatment and to a significantly shorter survival of mice bearing tumors expressing sgRNAs NT4 and T6, compared with Gal4-negative control tumors (Fig. 3*K* and *SI Appendix*, Fig. S10). Importantly, the expression of dCas9-VP64

with a nontargeting sgRNA did not have any significant influence on survival if compared with the transplantation of nontransduced cells, indicating that this system can be used in syngeneic immune-competent in vivo experiments without fundamentally interfering with disease kinetics per se (*SI Appendix*, Fig. S11). Thus, the fusion of dCas9 to the transcriptional activator VP64 can be used to strongly increase expression levels of MGMT and can rapidly model the influence of genetic alterations on treatment relapse an immune-competent model system in vivo.

RNAseq Demonstrates CRISPRi Has Negligible Off-Target Effects. It has been shown via ChIP-Seq that dCas9 binds to a significant number of off-target sites (46, 47). However, it is not known whether these mere interactions have any functional relevance and harbor the potency to cause off-target gene expression changes. Thus, we wanted to determine how prone our dCas9 system is to off-target effects. To address this question, we used our two best *Trp53* sgRNAs, T2 and T3, in conjunction with tumor cells derived from the well-established $Kras^{LSL\text{-}G12D/+}$; $p53^{fl/fl}$ lung adenocarcinoma transgenic mouse model (48). In this model, after Cre-lox recombination, the genomic binding sites for both sgRNAs are maintained, whereas several downstream *Trp53* coding exons are deleted, abolishing TRP53's ability to engage downstream effector pathways (Fig. 4*A*). Thus, any changes in gene expression induced by *Trp53* sgRNAs can be considered off target. As a control, we also included a negative control sgRNA, Gal4, which lacks any predicted matches in the mouse genome. We first confirmed that we could achieve dCas9-mediated knockdown in this cell line by targeting and successfully suppressing *Rev3l* transcription (*SI Appendix*, Fig. S12). We next performed RNAseq and compared the transcriptomes of cells either transduced with *Trp53* sgRNAs T2/T3 or with the control Gal4 sgRNA. To determine whether consistent gene expression changes between the three groups might be strong enough to cluster them next to one another, we conducted unsupervised hierarchical clustering (Fig. 4*B*). We saw that instead of clustering by sgRNA, clustering occurred by the biological replicate, suggesting that the observed expression differences between sgRNAs were minimal. To better quantify potential off-target transcript changes, we searched for significantly different transcripts among the three sgRNAs across all replicates. A mere three (Gal4 vs. *Trp53* T2) and one (Gal4 vs. *Trp53* T3) transcripts were identified to be significantly differentially expressed [$P < 0.01$

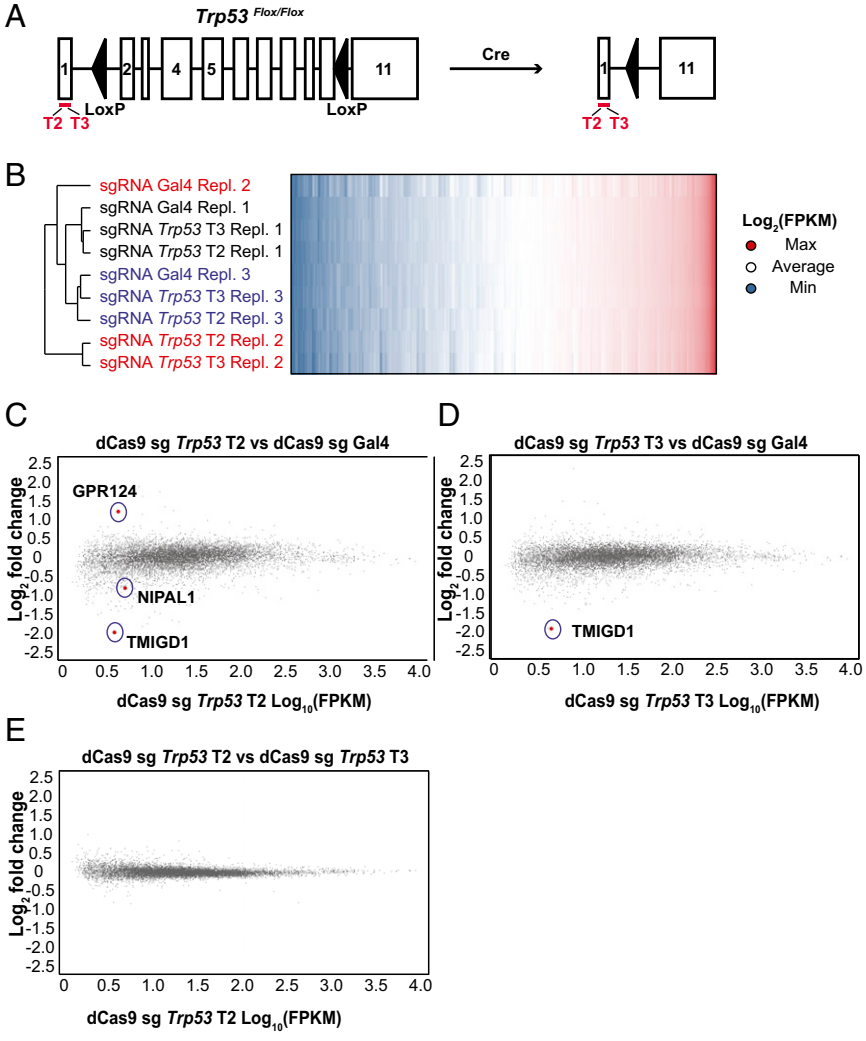

Fig. 4. CRISPRi knockdown is specific with minimal off-target effects. (*A*) A schematic showing that exons 2–10 of *Trp53* are lost after Cre-mediated recombination in $Kras^{LSL\text{-}G12D/+}$; $Trp53^{fl/fl}$ (KP) murine lung adenocarcinoma cells allowing a binding of both T2 and T3 *Trp53* sgRNAs without interfering with TRP53's downstream effects. (*B*) Hierarchical clustering of KP cells stably transduced with dCas9 and either sgRNAs targeting Gal4 (nontargeting control), *Trp53* T2 or *Trp53* T3. Text is colored by replicate. MA plots of genome-wide RNAseq data with significantly differentially regulated transcripts highlighted in red ($P < 0.01$ after FDR adjustment) for *Trp53* T2 vs. Gal4 (*C*), *Trp53* T3 vs. Gal4 (*D*), and *Trp53* T2 vs. *Trp53* T3 (*E*).

after false-discovery rate (FDR) adjustment] (Fig. 4 *C* and *D*). We were not able to identify any differentially expressed transcripts between T2 and T3 *Trp53* sgRNAs (Fig. 4*E*). This result may indicate that the lack of a perfectly matched binding site for the Gal4 sgRNA permits a small level of binding promiscuity that is not present for the *Trp53* sgRNAs, for which perfect genomic matches exist. Although the average number of reads aligning to *Trp53* were lower for both T2 and T3 in relation to Gal4, this decrease was not significant (*SI Appendix*, Fig. S13).

The Position Relative to the TSS, Not the Functional Protein Domain Associated with dCas9, Dictates the Direction of Transcriptional Regulation. Given the ability of dCas9 to activate and repress target gene expression, we were interested in determining whether a single construct would be capable of both activating and deactivating gene transcription. We therefore targeted either dCas9 alone or dCas9 linked to VP64 to different genomic regions around the TSS of both *Trp53* and *Mgmt* in ALL cells (Fig. 5*A*). As shown before for Eμ-*Myc p19*$^{Arf-/-}$ cells, dCas9 targeted to a genomic region downstream of *Trp53*'s TSS led to a potent decrease of transcript levels. Surprisingly, almost the same level of TRP53 suppression could be achieved when dCas9-VP64 was targeted to the same location (Fig. 5*B*). This finding suggests that VP64 loses its activating capability if targeted downstream of the TSS, and the associated dCas9 acts as a transcriptional roadblock that interferes with transcriptional elongation. In contrast, targeting dCas9-VP64 to a genomic region upstream of the TSS of *Mgmt* led to a potent transcriptional activation, but targeting dCas9 to this region caused a significant decrease of MGMT mRNA levels, suggesting an interference with transcriptional initiation (Fig. 5*B*). To determine the generalizability of the ability of dCas9-VP64 to repress transcription, we created 17 additional sgRNAs targeting the genomic region downstream of the corresponding TSSs of four more genes. For each gene, with five or fewer sgRNAs, we were able to achieve substantial transcriptional inhibition, ranging from 30 to 60% (Fig. 5*C*). Additionally, none of the sgRNAs elicited mRNA up-regulation of their respective target genes (*SI Appendix*, Fig. S14). This approach was also

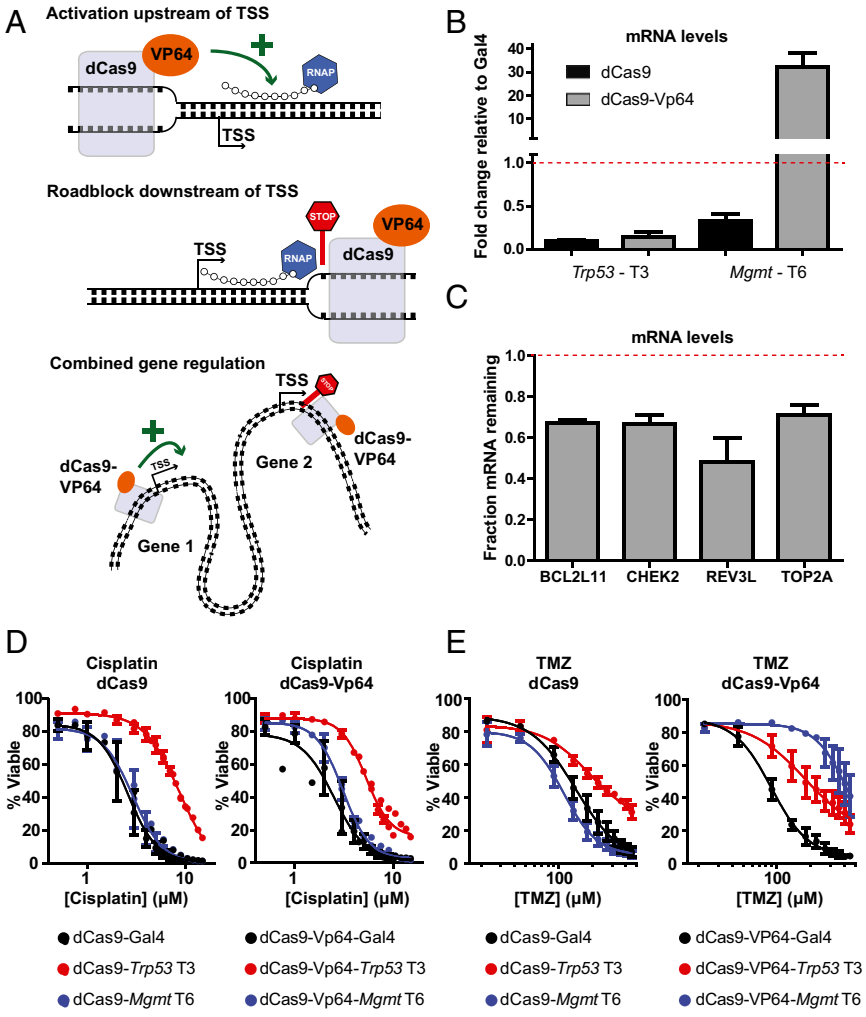

Fig. 5. The genomic binding region relative to the TSS determines gene activation or repression by dCas9. (*A*) A schematic overview showing dCas9-VP64 acting as either an activator or inhibitor of gene transcription. (*B*) TRP53 mRNA levels assessed by qRT-PCR in B-ALL cells transduced with either dCas9 or dCas9-VP64 and sgRNAs targeting Gal4 (negative control), *Trp53* T2, or *Mgmt* T6. Data are represented as mean ± SEM. (*C*) mRNA levels assessed by qRT-PCR in B-ALL cells transduced with dCas9-VP64 and sgRNAs targeting genomic regions downstream of the TSS. Data are represented as mean ± SEM. (*D*) Dose–response curves of B-ALL cells transduced with dCas9 or dCas9-VP64 and sgRNAs Gal4, *Trp53* T3, or *Mgmt* T6 doses with cisplatin. For both dCas9 and dCas9-VP64, logIC50's are significantly different at $P < 0.0001$ by an extra sum-of-squares *F* test. (*E*) Dose–response curves of B-ALL cells transduced with dCas9 or dCas9-VP64 and sgRNAs Gal4, *Trp53* T3, or *Mgmt* T6 doses with TMZ. For both dCas9 and dCas9-VP64, logIC50's are significantly different at $P < 0.01$ by an extra sum-of-squares *F* test.

successful in a human glioblastoma cell line, T98G, in which each of the sgRNAs tested elicited knockdown of MGMT (*SI Appendix*, Fig. S15). To explore whether these transcriptional effects translate into functional phenotypes, we treated ALL cells with either cisplatin (Fig. 5*D*) or temozolomide (Fig. 5*E*). As predicted by the changes in transcript levels, both dCas9 and dCas9-VP64 targeted to exon 1 of *Trp53* revealed resistance phenotypes to both cisplatin and temozolomide treatment (Fig. 5 *D* and *E*). In contrast, only the activation of *Mgmt* transcription by dCas9-VP64 led to cellular resistance to temozolomide. To further demonstrate the robustness of dCas9-VP64–mediated knockdown, we targeted *Rev3l*, the catalytic subunit of the translesion polymerase Pol ζ. Whereas the transcriptional repression of *Rev3l* is not expected to confer a selective growth advantage to cells, lack of *Rev3l* sensitizes to cisplatin treatment (49, 50). Indeed, all sgRNAs targeting *Rev3l* significantly sensitized dCas9-VP64 ALL cells to cisplatin treatment (*SI Appendix*, Fig. S16). We therefore concluded that a dCas9 construct with a linked VP64 transcriptional activation domain can be used for both transcriptional activation and repression, depending on its relative position to the TSS. Thus, CRISPRi and CRISPRa can be performed interchangeably using the same dCas9 protein simply by altering the targeted DNA location in respect to the corresponding TSS.

A Pooled in Vivo Gene Activation Screen Identifies Novel Mediators of Bone Marrow Treatment Relapse in B-ALL. The construction of large open-reading frame (ORF) libraries has made it possible to screen for gain-of-function phenotypes (51); however, creation of these libraries remains expensive and difficult. We were interested in determining whether our Cas9-VP64–based system was robust enough to perform pooled in vitro and in vivo pooled screens. We therefore constructed a small sgRNA library targeting 25 known or putative regulators of the DNA damage response upstream of the TSS with a coverage of 5 sgRNAs per gene and 50 additional nontargeting negative control sgRNAs (*SI Appendix*, Fig. S17). The library was transduced into dCas9-VP64–expressing B-ALL cells, and infected cells were purified by flow cytometry-based sorting. SgRNA-expressing cells were injected into syngeneic recipient mice or maintained in culture (Fig. 6*A*). Upon disease onset, mice and cells were treated in parallel with TMZ or vehicle. After disease relapse, we isolated tumor cells from the bone marrow of leukemic mice and extracted genomic DNA from both the in vitro and the in vivo samples. Genomic insertions were amplified by PCR, and the sgRNA representation was deconvoluted via high-throughput sequencing. Sequencing reactions did not bias sgRNA quantification, and we were able to detect most sgRNAs at more than 500 reads per sgRNA in both the in vitro and in vivo samples (Fig. 6*B* and *SI Appendix*, Fig. S18). We next sought to identify sgRNAs that impacted the cellular sensitivity to TMZ by comparing the relative representation of each sgRNA in the TMZ-treated group to its representation in the vehicle group and generating a log(fold-change) value for each sgRNA (Dataset S1). Using the negative control guide population as a null distribution, we were able to assess significance levels of the observed fold change effects either for single sgRNAs or on the gene level by examining the effects of multiple sgRNA molecules targeting the same gene. As expected, transcriptional activation of *Mgmt* was identified to be the most potent resistance factor to TMZ chemotherapy in vitro and in vivo (Fig. 6 *C* and *D*). Interestingly, transcriptional activation of Checkpoint kinase 2 (*Chek2*), a major signaling component of the DNA damage response network (52), was identified as causing sensitivity to TMZ and slowing down disease progression upon gene induction both in vitro and in vivo (*SI Appendix*, Fig. S19). We therefore performed validation experiments for two independent sgRNAs (Chek2-2 and Chek2-5) in vivo. Closely matching our screen-based prediction, we found CHEK2 up-regulation (*SI Appendix*, Fig. S20) extended survival in the absence of treatment (Fig. 6*E*) and delayed disease relapse after TMZ treatment (Fig. 6*F*) compared with control mice without dCas9 targeted to the Chek2 genomic locus.

Discussion

This study describes an approach to dCas9-mediated gene level perturbation that represents a robust, specific, and tractable tool for modeling cancer progression and therapeutic relapse both in vitro and in syngeneic immune-competent mouse models in vivo. The guided genomic targeting of dCas9 along with the transcription activating protein domain VP64 allows for the rapid and inexpensive modeling of both gene activation and inactivation phenotypes in one sgRNA per gene settings or in multiplexed pooled screens. Thus, dCas9-mediated gene level changes represent an attractive tool for both functional validation experiments and for unbiased screening approaches. Additionally, because dCas9 does not generate different genetic entities in each individual cell, its use circumvents the requirement of the artifact-prone generation of single cell clones, as often needed for Cas9-based studies.

Our in vivo gene activation screen identified *Chek2*, a serine threonine kinase and candidate tumor suppressor gene, as delaying both progression and therapeutic relapse of B-ALL in vivo upon transcriptional activation. Notably, certain inactivating or protein-destabilizing mutations of the human *CHEK2* gene have been implicated in the development of multiple cancers (especially breast and prostate) (53). Furthermore, CHEK2 expression is frequently reduced in cancer cell lines (54). Oncogenic stress or DNA lesions can cause an activation of CHEK2, which is then capable of driving cells into apoptosis mediated by TP53 (55). High levels of CHEK2 in tumor cell lines are frequently associated with the inactivation of p53 (54). Here, we demonstrate that the transcriptional activation of *Chek2* in the presence of a wild-type TRP53 is capable of slowing down tumor progression and sensitizing to chemotherapy. It remains to be explored whether this phenotype is exclusive to tumor cells without inactivation of TRP53.

Interestingly, we observed some discordance in the amounts of mRNA and protein up-regulation for MGMT following CRISPRa. It is unclear whether this discordance represents a universal effect connected to the activation of the endogenous transcription machinery as opposed to overexpression of a codon-optimized and virally introduced gene coding sequence.

One key feature of dCas9-mediated transcriptional activation is the ability to rapidly and cost-effectively generate large sgRNA libraries. This finding stands in contrast to the construction of cDNA/ORF libraries, which, because of extreme heterogeneity in gene length, are protracted and expensive undertakings. Here, we demonstrate, for the first time to our knowledge, that gene activation screens based on CRISPRa, detecting both sgRNA enrichment and depletion, are feasible in vivo and can obviate many of the technical bottlenecks of gene overexpression screens in mouse models of cancer.

The construction of a Cre-dependent Rosa26 Cas9 knock-in mouse has recently helped to decrease delivery vector sizes and to make in vivo genome editing of nontumor cells possible, even if they are located in anatomical loci that are hard to access (56). The combination of this approach along with dCas9-based in vivo functionality should allow for the study of gene activation phenotypes in diverse and physiologically relevant contexts; this includes pooled screens for genetic factors of organ development, as has been demonstrated in a genome-wide fashion using RNAi (57).

Importantly, the scarcity of transcriptional alterations in our dCas9 control experiments suggests that CRISPRa screening may not be encumbered by significant off-target effects. This finding is perhaps unexpected given Cas9's promiscuous binding to many genomic loci in published Chip-Seq data (46, 47) and suggests that the vast majority of these off-target genome–Cas9 interactions are functionally irrelevant. Thus, data from pooled dCas9 screens may be much easier to deconvolute than expected, and that the rate of false-positive screening hits may be quite low relative to other screening approaches.

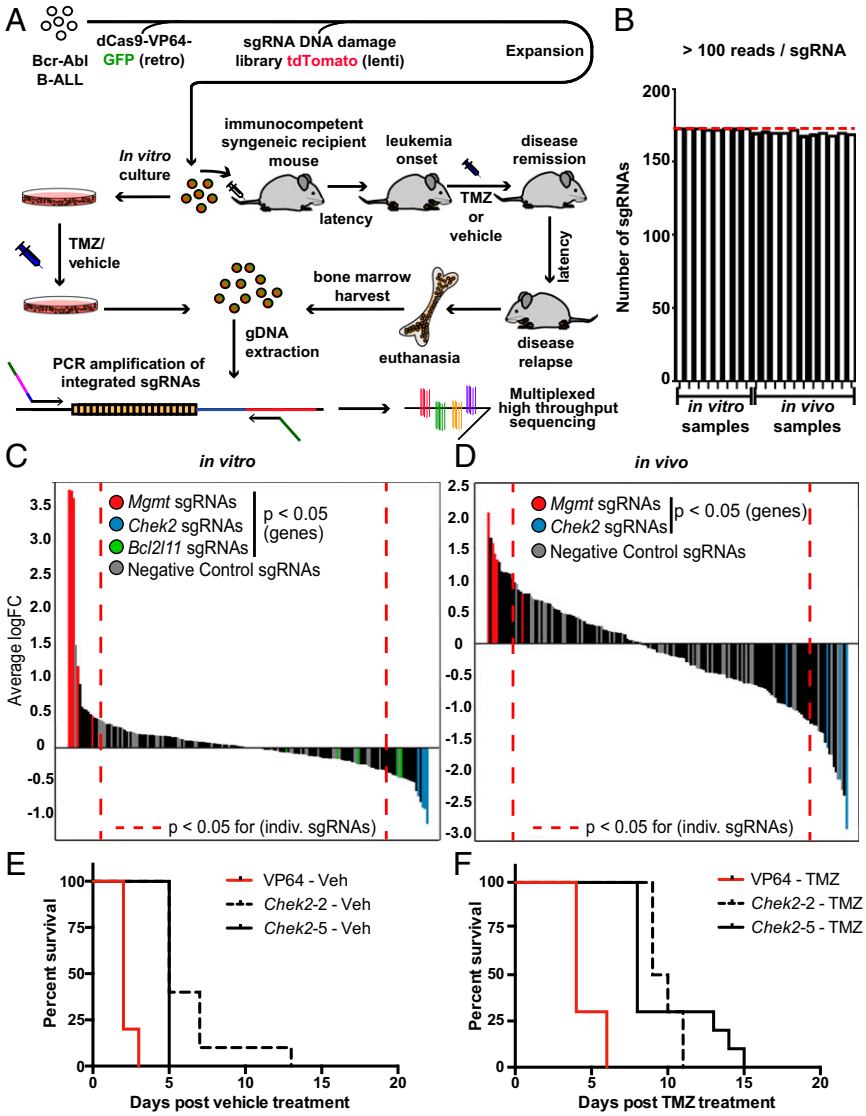

Fig. 6. Parallel in vitro and in vivo dCas9-VP64–mediated gene activation screens for mediators of leukemia treatment relapse reveal opposing effects of MGMT and CHEK2 on temozolomide sensitivity. (*A*) A diagram of the in vitro and in vivo screening strategies. (*B*) A graph showing the number of unique sgRNAs detected in in vitro and in vivo samples. In vitro (*C*) and in vivo (*D*) log10 fold-change plots showing sgRNA representation after treatment. sgRNAs of statistically significant genes are shown in color. (*E*) Overall survival without treatment with and without *Chek2* transcriptional activation. Via log-rank test, $P < 0.0001$ between both VP64 vs. *Chek2*-2 and VP64 vs. *Chek2*-5. (*F*) Overall survival after TMZ treatment with and without Chek2 transcriptional activation. Via log rank test, $P < 0.0001$ between both VP64 vs. Chek2-2 and VP64 vs. Chek2-5 (mouse numbers: dCas9 + sgGal4 vehicle $n = 10$, dCas9 + sgGal4 TMZ $n = 10$, dCas9 + sg*Chek2*-2 vehicle $n = 10$, dCas9 + sg*Chek2*-2 TMZ $n = 10$, dCas9 + sg*Chek2*-5 vehicle $n = 10$, dCas9 + sg*Chek2*-5 $n = 10$).

Materials and Methods

Vector Generation and sgRNA Library Cloning. dCas9 fused to two C-terminal SV40 NLSs was derived from pHR-SFFV-dCas9-BFP (32) (see *SI Appendix, SI Materials and Methods* for cloning strategies). sgRNAs were cloned into U6-sgRNA-CMV-tdTomato as described (30) (targeted genomic sequences can be found in *SI Appendix*, Table S1). Construction of the screen library is described in *SI Appendix*, Fig. S17.

Cell Culture. *Eμ-Myc p19$^{Arf-/-}$* mouse B-cell lymphomas were cultured in B-cell medium (45% DMEM/45% IMDM/10% FBS, supplemented with 2 mM L-glutamine and 5 μM β-mercaptoethanol). *Bcr-Abl*–driven mouse B-ALL leukemia cells (58) were cultured in RPMI supplemented with 10% FBS, 4 mM L-glutamine, and 5 μM β-mercaptoethanol. Lung adenocarcinoma cells (KP cells) had been derived from *Kras$^{LSL-G12D}$ p53^{fl}* mice after Cre-mediated recombination and tumor onset (48) and were cultured in DMEM complete medium (90% DMEM/10% FBS). T98G cells were purchased from ATCC (CRL-1690) and cultured in DMEM complete medium (90% DMEM/10% FBS). See *SI Appendix, SI Materials and Methods* for virus production, drug treatment, and flow cytometry.

RNA Interference. The shRNA targeting p53 was expressed in a mir30 context as described (59) targeting the following mRNA sequence: CCACTACAAGTACATGTGTAA.

Total RNA Purification, cDNA Synthesis, and qRT-PCR. Total RNA was isolated by using the NucleoSpin RNA kit (Machery-Nagel). To quantify gene expression levels, equal amounts of cDNA were synthesized by using the PrimeScript RT reagent Kit with gDNA Eraser (Takara), mixed with the Fast SYBR Green Mastermix (Applied Biosystems), and gene expression was analyzed with a StepOnePlus Real-Time PCR System (Applied Biosystems). Primer sequences are listed in *SI Appendix*, Table S2. The number of cycles required to cross a fluorescence threshold (C_T value) was noted for each transcript and normalized to GAPDH.

RNAseq. See *SI Appendix, SI Materials and Methods* for RNA extraction, library preparation, sequencing, and analysis. In brief, DESeq was used to determine FDR-adjusted *P* values for transcripts that were significantly differentially expressed. Transcripts that did not pass the expression threshold

of >0.2 fragments per kilobase of fragment per million mapped reads and a variability threshold of >0.2 SD across replicates were eliminated from analysis.

Western Blot. Protein extracts, separated by SDS/PAGE and transferred onto PVDF membranes, were probed with antibodies against stated proteins. See *SI Appendix, SI Materials and Methods* for antibody list and visualization method.

Transplantation of Eμ-Myc p19$^{Arf-/-}$ or B-ALL Cells into Immune-Competent Syngeneic Mice and in Vivo Drug Treatment. Six-week-old female C57BL/6J mice were purchased from the Jackson Laboratory (stock no. 000664); 2×10^6 cells per mouse were transplanted by tail-vein injection in 200 μL of PBS. All mouse experiments were approved by Massachusetts Institute of Technology's Committee on Animal Care prior to execution. See *SI Appendix, SI Materials and Methods* for drug treatment.

In Vitro and in Vivo sgRNA Screen. Briefly, B-ALL cells were first infected with both dCas9-VP64 and a custom sgRNA library [targeting the genomic DNA region upstream of the TSS of genes previously implicated into the response to DNA damage (125 sgRNAs targeting genomic DNA regions and 50 negative control sgRNAs)]. See Fig. 6*A* and *SI Appendix, SI Materials and Methods* for screening strategy and experimental details.

ACKNOWLEDGMENTS. We thank Charlie Whitaker, Jie Wu, Stuart Levine, Glen Paradis, and the Koch Institute Flow Cytometry core for advice and services; and Eric Bent, Ian Cannell, Silvia Fenoglio, Bert van de Kooij, Karl Merrick, and Boyang Zhao for thoughts and comments on the manuscript. Funding for this study was provided by Integrative Cancer Biology Program Grant U54-CA112967-06 and Koch Institute Support (core) Grant P30-CA14051 from the National Cancer Institute. C.J.B. is the recipient of a Mildred-Scheel Fellowship of the German Cancer Foundation.

1. Pettersson E, Lundeberg J, Ahmadian A (2009) Generations of sequencing technologies. *Genomics* 93(2):105–111.
2. Alexandrov LB, et al.; Australian Pancreatic Cancer Genome Initiative; ICGC Breast Cancer Consortium; ICGC MMML-Seq Consortium; ICGC PedBrain (2013) Signatures of mutational processes in human cancer. *Nature* 500(7463):415–421.
3. Lawrence MS, et al. (2013) Mutational heterogeneity in cancer and the search for new cancer-associated genes. *Nature* 499(7457):214–218.
4. Roberts SA, Gordenin DA (2014) Hypermutation in human cancer genomes: Footprints and mechanisms. *Nat Rev Cancer* 14(12):786–800.
5. Carroll D (2011) Genome engineering with zinc-finger nucleases. *Genetics* 188(4):773–782.
6. Kim YG, Cha J, Chandrasegaran S (1996) Hybrid restriction enzymes: Zinc finger fusions to Fok I cleavage domain. *Proc Natl Acad Sci USA* 93(3):1156–1160.
7. Boch J (2011) TALEs of genome targeting. *Nat Biotechnol* 29(2):135–136.
8. Gaj T, Gersbach CA, Barbas CF, 3rd (2013) ZFN, TALEN, and CRISPR/Cas-based methods for genome engineering. *Trends Biotechnol* 31(7):397–405.
9. Sander JD, Joung JK (2014) CRISPR-Cas systems for editing, regulating and targeting genomes. *Nat Biotechnol* 32(4):347–355.
10. Doudna JA, Charpentier E (2014) The new frontier of genome engineering with CRISPR-Cas9. *Science* 346(6213):1258096–1258096.
11. Shalem O, et al. (2014) Genome-scale CRISPR-Cas9 knockout screening in human cells. *Science* 343(6166):84–87.
12. Wang T, Wei JJ, Sabatini DM, Lander ES (2014) Genetic screens in human cells using the CRISPR-Cas9 system. *Science* 343(6166):80–84.
13. Koike-Yusa H, Li Y, Tan E-P, Velasco-Herrera MdelC, Yusa K (2014) Genome-wide recessive genetic screening in mammalian cells with a lentiviral CRISPR-guide RNA library. *Nat Biotechnol* 32(3):267–273.
14. Zhou Y, et al. (2014) High-throughput screening of a CRISPR/Cas9 library for functional genomics in human cells. *Nature* 509(7501):487–491.
15. Chen S, et al. (2015) Genome-wide CRISPR screen in a mouse model of tumor growth and metastasis. *Cell* 160(6):1246–1260.
16. Engelman JA, et al. (2007) MET amplification leads to gefitinib resistance in lung cancer by activating ERBB3 signaling. *Science* 316(5827):1039–1043.
17. Bean J, et al. (2007) MET amplification occurs with or without T790M mutations in EGFR mutant lung tumors with acquired resistance to gefitinib or erlotinib. *Proc Natl Acad Sci USA* 104(52):20932–20937.
18. Turke AB, et al. (2010) Preexistence and clonal selection of MET amplification in EGFR mutant NSCLC. *Cancer Cell* 17(1):77–88.
19. Yano S, et al. (2008) Hepatocyte growth factor induces gefitinib resistance of lung adenocarcinoma with epidermal growth factor receptor-activating mutations. *Cancer Res* 68(22):9479–9487.
20. Curt GA, et al. (1983) Unstable methotrexate resistance in human small-cell carcinoma associated with double minute chromosomes. *N Engl J Med* 308(4):199–202.
21. Camgoz A, Gencer EB, Ural AU, Baran Y (2013) Mechanisms responsible for nilotinib resistance in human chronic myeloid leukemia cells and reversal of resistance. *Leuk Lymphoma* 54(6):1279–1287.
22. Sun C, et al. (2014) Reversible and adaptive resistance to BRAF(V600E) inhibition in melanoma. *Nature* 508(7494):118–122.
23. Temple G, et al.; MGC Project Team (2009) The completion of the Mammalian Gene Collection (MGC). *Genome Res* 19(12):2324–2333.
24. Tanenbaum ME, Gilbert LA, Qi LS, Weissman JS, Vale RD (2014) A protein-tagging system for signal amplification in gene expression and fluorescence imaging. *Cell* 159(3):635–646.
25. Gilbert LA, et al. (2013) CRISPR-mediated modular RNA-guided regulation of transcription in eukaryotes. *Cell* 154(2):442–451.
26. Gilbert LA, et al. (2014) Genome-scale CRISPR-mediated control of gene repression and activation. *Cell* 159(3):647–661.
27. Mali P, et al. (2013) CAS9 transcriptional activators for target specificity screening and paired nickases for cooperative genome engineering. *Nat Biotechnol* 31(9):833–838.
28. Perez-Pinera P, et al. (2013) RNA-guided gene activation by CRISPR-Cas9-based transcription factors. *Nat Methods* 10(10):973–976.
29. Cheng AW, et al. (2013) Multiplexed activation of endogenous genes by CRISPR-on, an RNA-guided transcriptional activator system. *Cell Res* 23(10):1163–1171.
30. Maeder ML, et al. (2013) CRISPR RNA-guided activation of endogenous human genes. *Nat Methods* 10(10):977–979.
31. Konermann S, et al. (2015) Genome-scale transcriptional activation by an engineered CRISPR-Cas9 complex. *Nature* 517(7536):583–588.
32. Qi LS, et al. (2013) Repurposing CRISPR as an RNA-guided platform for sequence-specific control of gene expression. *Cell* 152(5):1173–1183.
33. Schmitt CA, McCurrach ME, de Stanchina E, Wallace-Brodeur RR, Lowe SW (1999) INK4a/ARF mutations accelerate lymphomagenesis and promote chemoresistance by disabling p53. *Genes Dev* 13(20):2670–2677.
34. Vousden KH, Prives C (2009) Blinded by the light: The growing complexity of p53. *Cell* 137(3):413–431.
35. Brady CA, Attardi LD (2010) p53 at a glance. *J Cell Sci* 123(Pt 15):2527–2532.
36. Bieging KT, Mello SS, Attardi LD (2014) Unravelling mechanisms of p53-mediated tumour suppression. *Nat Rev Cancer* 14(5):359–370.
37. Evan GI, Vousden KH (2001) Proliferation, cell cycle and apoptosis in cancer. *Nature* 411(6835):342–348.
38. Lutzker SG, Mathew R, Taller DR (2001) A p53 dose-response relationship for sensitivity to DNA damage in isogenic teratocarcinoma cells. *Oncogene* 20(23):2982–2986.
39. Fellmann C, et al. (2011) Functional identification of optimized RNAi triggers using a massively parallel sensor assay. *Mol Cell* 41(6):733–746.
40. Wang D, et al. (2015) Adenovirus-mediated somatic genome editing of Pten by CRISPR/Cas9 in mouse liver in spite of Cas9-specific immune responses. *Hum Gene Ther* 26(7):432–442.
41. Seipel K, Georgiev O, Schaffner W (1992) Different activation domains stimulate transcription from remote ('enhancer') and proximal ('promoter') positions. *EMBO J* 11(13):4961–4968.
42. Pegg AE, Dolan ME, Moschel RC (1995) Structure, function, and inhibition of O6-alkylguanine-DNA alkyltransferase. *Prog Nucleic Acid Res Mol Biol* 51:167–223.
43. Hegi ME, et al. (2005) MGMT gene silencing and benefit from temozolomide in glioblastoma. *N Engl J Med* 352(10):997–1003.
44. Medeiros BC, et al. (2012) Tailored temozolomide therapy according to MGMT methylation status for elderly patients with acute myeloid leukemia. *Am J Hematol* 87(1):45–50.
45. Brandwein JM, et al. (2014) Phase II study of targeted therapy with temozolomide in acute myeloid leukaemia and high-risk myelodysplastic syndrome patients pre-screened for low O(6)-methylguanine DNA methyltransferase expression. *Br J Haematol* 167(5):664–670.
46. Wu X, et al. (2014) Genome-wide binding of the CRISPR endonuclease Cas9 in mammalian cells. *Nat Biotechnol* 32(7):670–676.
47. Kuscu C, Arslan S, Singh R, Thorpe J, Adli M (2014) Genome-wide analysis reveals characteristics of off-target sites bound by the Cas9 endonuclease. *Nat Biotechnol* 32(7):677–683.
48. Jackson EL, et al. (2005) The differential effects of mutant p53 alleles on advanced murine lung cancer. *Cancer Res* 65(22):10280–10288.
49. Xie K, Doles J, Hemann MT, Walker GC (2010) Error-prone translesion synthesis mediates acquired chemoresistance. *Proc Natl Acad Sci USA* 107(48):20792–20797.
50. Doles J, et al. (2010) Suppression of Rev3, the catalytic subunit of Polzeta, sensitizes drug-resistant lung tumors to chemotherapy. *Proc Natl Acad Sci USA* 107(48):20786–20791.
51. Yang X, et al. (2011) A public genome-scale lentiviral expression library of human ORFs. *Nat Methods* 8(8):659–661.
52. Reinhardt HC, Yaffe MB (2009) Kinases that control the cell cycle in response to DNA damage: Chk1, Chk2, and MK2. *Curr Opin Cell Biol* 21(2):245–255.
53. Nevanlinna H, Bartek J (2006) The CHEK2 gene and inherited breast cancer susceptibility. *Oncogene* 25(43):5912–5919.
54. Zoppoli G, et al. (2012) CHEK2 genomic and proteomic analyses reveal genetic inactivation or endogenous activation across the 60 cell lines of the US National Cancer Institute. *Oncogene* 31(4):403–418.
55. Bartkova J, et al. (2005) DNA damage response as a candidate anti-cancer barrier in early human tumorigenesis. *Nature* 434(7035):864–870.
56. Platt RJ, et al. (2014) CRISPR-Cas9 knockin mice for genome editing and cancer modeling. *Cell* 159(2):440–455.
57. Beronja S, et al. (2013) RNAi screens in mice identify physiological regulators of oncogenic growth. *Nature* 501(7466):185–190.
58. Williams RT, Roussel MF, Sherr CJ (2006) Arf gene loss enhances oncogenicity and limits imatinib response in mouse models of Bcr-Abl-induced acute lymphoblastic leukemia. *Proc Natl Acad Sci USA* 103(17):6688–6693.
59. Dickins RA, et al. (2005) Probing tumor phenotypes using stable and regulated synthetic microRNA precursors. *Nat Genet* 37(11):1289–1295.